Improvements to rational surface analysis in toroidal magnetic confinement fields

Jacob Van Alstyne
University of Utah

December 2012

Abstract

Magnetic confinement fusion is an advanced technology under investigation as a potential low cost source of energy. Progress in this area depends upon the ability of researchers to understand the magnetic field containing the fusion plasma. In previous work done by Sanderson, Chen, Trichoche, et al [1], topological features of the toroidal magnetic field are identified by analyzing the Poincaré map of sampled fieldlines. In this work, we take a look at a particular class of periodic fieldlines that are characteristic of rational surfaces. As a result of their unique periodicity and unlike their quasi-periodic counterparts, they do not spread out across the magnetic surface. Therefore, the number of data points on the cross-sectional curve in the Poincaré section is limited to the toroidal winding number of the surface. The result is a piecewise linear approximation of the surface the degree of which, unlike irrational surfaces, can not be improved by increasing the number of puncture points. Because of the scarcity of information from a single fieldline on rational surfaces (esp. low order), it would benefit researchers to be able to increase the number of fieldlines on the surface to more accurately represent the surface profile in the Poincaré section. In order to do this, a strategy based on seeding fieldlines between puncture points on a rational surface and minimizing their winding distances using a known numerical search technique has been implemented and deployed in C++ as a plugin to the VisIt visualization toolset [2]. A complete discussion of this strategy and the results are contained within this paper.

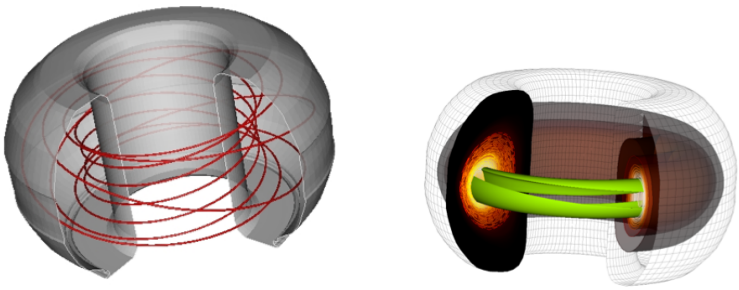

Figure 1: **Left:** A profile of the DIII-D Tokomak and a single quasi-periodic magnetic field, shown as red curves. **Right:** A visualization of a magnetic confinement fusion simulation showing an *island chain* surface in green. **Both:** Images borrowed with permission [1]

1 Introduction

Researchers wanting to harness the power of nuclear fusion must somehow confine the hot plasma containing the reaction. One of the most promising techniques for stabilizing the fusion plasma is a toroidal magnetic field inside a device known as a tokomak reactor (see Figure 1). In order to succeed, the magnetic field must realize a condition such that its fieldlines travel in a helical pattern around the torus. Researchers study the results of numerical simulations as a way to designing better reactors and must therefore characterize the orbits of the fieldlines. A technique for analyzing the magnetic fields numerically, as described by Sanderson, et al [1] involves the use of a Poincaré map as a way of reducing the Hamiltonian dimensionality of the simulation. A collection of points formed from a certain number of intersections of the fieldlines with a plane perpendicular to the toroidal axis gives a complete representation of the toroidal magnetic field, and an analysis of the puncture points yields details about the characteristics of the orbits. Periodic fieldlines of closed finite length are found on rational surfaces (see Figure 3), while quasi-periodic fieldlines (see Figure 2) will travel infinitely over irrational surfaces.

Following on the work of Sanderson, et al [1], this work takes a deeper look at those fieldlines following their characterization through analysis as having a rational safety factor– indicative of a periodic fieldline on a rational surface. Specifically, the precise contours and shape of low order rational surfaces are not as easily known as that of their irrational counterparts. This is a consequence of the closed fieldlines of a rational surface that due to their nature don't spread out across the surface as they wind around the toroidal axis. Contrariwise, fieldlines on an irrational surface puncture the toroidal plane in a progressive manner, intersecting the plane at an offset from the previous intersection of the same winding group. This does not hold for rational surfaces, where each

intersection of the same toroidal winding number occurs in the same place as the last within precision (see Figure 5), yielding no new information. However, more information is desired since rational surfaces tend to break up first into island chains as a response to perturbations in the field, overall increasing the chaos and decreasing the stability of the confinement.

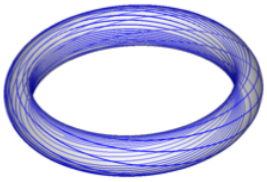

Figure 2: The quasi-periodic fieldlines typical of an irrational surface. [1]

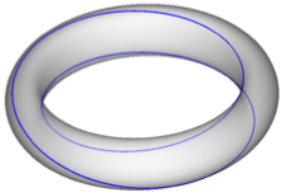

Figure 3: A rational surface with a periodic fieldline. [1]

Figure 4: An island chain. [1]

In the interest of filling in the gaps between the otherwise somewhat sparse Poincaré punctures from a rational fieldline, a numerical search based on a well known [3] minimization technique has been designed to search out points lying on the surface between those already discovered. The idea is to generate enough new points on the surface to compensate for the fact the original points didn't spread out and reveal the surface through their own natural drift (see Figure 6).

This concept has been deployed as an extension to an existing library of mostly C++ code which can be leveraged inside a number of visualization packages such as VisIt and SCIRun. The main algorithm starts with the puncture points of a rational surface, and based on the euclidean spacing of those field lines in a cross sectional plane of the torus, new fieldlines are spawned in a pattern strategically designed to leverage the monotonicity of the local vector field data to locate and draw new points lying directly on the surface. The numerical search is based on a simple bracketing and minimization routine [3].

The resultant rendering of the surface profile more precisely represents the rational surface and can provide an arbitrary level of detail depending on the number and spacing of the initial seeds.

2 Background

2.1 Vector Fields

Toroidal magnetic fields are described mathematically as divergence-free pseudo-vector fields. A vector field $\mathcal{V}$ on a manifold $\mathcal{M}$ expressible as an ordinary

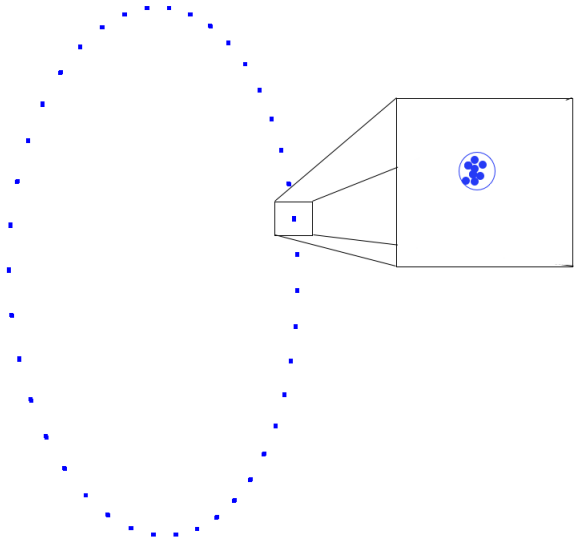

Figure 5: A Poincaré plot of a rational fieldline with a close-up of a puncture point composed of multiple intersections of the same toroidal winding group– the circle indicates the limit on precision. Notice that while the groups of points are not drawn connected, they nevertheless form a piecewise linear approximation of the surface profile.

differential equation $\frac{dx}{dt} = V(x)$ has a set of solutions that produce a *flow* over $\mathcal{M}$, or a continuous function $\varphi(0,x) : \mathbb{R} \times \mathcal{M} \to \mathcal{M}$ such that $\varphi(0,x) = x, \forall x \in \mathcal{M}$ and $\frac{d\varphi}{dt}|_{t,x} = \mathcal{V}(\varphi(t,x)), \forall t \in \mathbb{R}$. A fieldline that passes through a point $x_0 \in \mathcal{M}$ is a curve on $\mathcal{M}$, since $x(\cdot) \equiv \varphi(\cdot, x_0)$. A fieldline through $x_0 \in \mathcal{M}$ is on a *periodic orbit* if $x(T) = x_0$ for some $T \in \mathbb{R}, T \neq 0$. A set $S \in \mathcal{M}$ is *invariant* if the flow returns it to itself. The periodic orbits we look at are invariant sets which can be analyzed using a Poincaré map.

If we have an orbit Γ of φ in an n dimensional manifold $\mathcal{M}$, and we let $\mathcal{T}$ be an $n-1$ dimensional cross section such that φ is everywhere transverse to $\mathcal{T}$, then $\mathcal{T}$ is called a Poincaré section. A puncture point on a Poincaré cross section is defined as an intersection of Γ with $\mathcal{T}$. This point is described by $p_i \in \mathcal{T} \cap \Gamma$ where $i \in \mathcal{N}$ denotes the intersection ordering.

2.2 Poincaré map

A Poincaré map in $\mathcal{T}$ is defined as $P : \mathbb{R} \times \mathcal{T} \to \mathcal{T}$, leading from puncture point p_i to p_{i+1} along the orbit Γ where $p_i, p_{i+1} \in \mathcal{T} \cap \Gamma$. In other words, $p_{i+1} = P(p_i) = \varphi(\tau, p_i)$ where $\tau \in \mathbb{R}$ and $\tau > 0$ is the time for Γ to travel from p_i to p_{i+1}. The collection of points generated in $\mathcal{T}$ is known as the *Poincaré*

plot of Γ. A Poincaré map is a well known technique for researching regions near periodic solutions to recurrent flows in dynamic systems [4].

2.3 Toroidal Magnetic Fields

Magnetic fieldlines traversing helically inside a toroidal containment device will wind around both the toroidal (major) axis and the poloidal (minor) axes of the torus. The ratio of the number of times the fieldline circumnavigates the toroidal axis for each rotation around the poloidal axis is known as the fieldline's *safety factor* or q. The safety factor is related to the stability of the confined plasma. It is defined by

$$q = \lim_{n_T \to +\infty} \frac{n_T}{\#_\theta(n_T)} \tag{1}$$

where n_T is the toroidal winding number, or the number of times a fieldline Γ intersects a poloidal cross section $\mathcal{T}$ and $\#_\theta(n_T)$ is the poloidal winding number, or the number of times Γ intersections the toroidal cross section at $z = 0$. The poloidal winding number is $\#_\theta(n_T)$ when Γ crosses the poloidal plane n_T times. Unless the fieldline is chaotic, the limit defined above exists.

An *irrational surface* produces quasi-periodic fieldlines (Figure 2) which spread across the surface resulting in an irrational q. These produce two different topologies in a Poincaré section, either a single closed curve or multiple closed curves. Single closed curves indicate a magnetic flux surface while multiple closed curves indicate a magnetic island chain (Figure 4) which usually results from the breakup of a *rational surface*. The number of islands matches n_T.

A rational surface produces fieldlines (Figure 3) which do not spread out over the surface, but which rather wind back onto themselves after the number of toroidal windings equals n_T. These fieldlines are indicated by a rational q. Aside from being the topic of this work, the importance of rational surfaces lies in the susceptibility of those fieldlines with low-order safety factors to breaking up into island chains in response to perturbations to the magnetic field, disrupting the confinement stability.

2.4 Error and Stability

A fieldline Γ is an approximated solution to the ordinary differential equation $\frac{dx}{dt} = f(x)$ with $x(0) = s, s \in \mathbb{R}$. It is assumed $f_x = \frac{\partial f}{\partial x}$ is continuous and satisfies $f_x(t, x) \leq \lambda$ for all $t \in [0, T]$ and all $x \in \mathbb{R}$. Numerical integration techniques such as the Adams-Bashforth multi-step method used to approximate values

$x(t)$ at time t necessarily introduce *local truncation errors* at each iteration which accumulate into *global truncation error*.

The formula for a k-step linear multi-step method is given by [5] as $a_k x_n + a_{k-1}x_{n-1} + \cdots + a_1 x_{n-k-1} + a_0 x_{n-k} = h[b_k f_n + b_{k-1}f_{n-1} + \cdots + b_1 f_{n-k+1} + b_0 f_{n-k}]$ which can also be written as $x_n = -\frac{1}{a_k}(a_{k-1}x_{n-1} + \cdots + a_1 n_{n-k-1} + a_0 x_{n-k}) + \frac{h}{a_k}[b_k f_n + b_{k-1}f_{n-1} + \cdots + b_1 f_{n-k+1} + b_0 f_{n-k}]$. This equation computes x_n from the k preceding values, $x_{n-k}, x_{n-k+1}, \cdots, x_{n-1}$. Convergence of a linear multi-step method in a region $[t_0, t_1]$ requires that $\lim_{h\to 0} x_h(t) = x(t), t \in [t_0, t_1]$. Here, $x_h(t)$ indicates the numerical solution computed at time t with a step size of h while $x(t)$ indicates the exact solution. Setting b_k to 0 makes the method *explicit*, since $f_n = f(t_n, x_n)$. The order of the method corresponds with the number of terms in the Taylor series expansion of the solution simulated by the method. To illustrate this better, rewrite the equation above as a linear functional $L[x] = \sum_{j=0}^{k}[a_j x(jh) - hb_j f(jh)] = \sum_{j=0}^{k}[a_j x(jh) - hb_j x'(jh)]$. Write x and x' as $x(jh) = \sum_{i=0}^{\infty}\frac{(jh)^i}{i!}x^{(i)}(0)$ and $x'(jh) = \sum_{i=0}^{\infty}\frac{(jh)^i}{i!}x^{(i+1)}(0)$ respectively. Apply these results to the linear functional to get $L[x] = \sum_{j=0}^{k}\left[a_j\sum_{i=0}^{\infty}\frac{(jh)^i}{i!}x^{(i)}(0) - hb_j\sum_{i=0}^{\infty}\frac{(jh)^i}{i!}x^{(i+1)}(0)\right]$. Collect terms proportional to $x(0), x'(0), \cdots$ to get $L[x] = d_0 x(0) + d_1 h x'(0) + d_2 h^2 x''(0) + \cdots$. The coefficients are $d_0 = \sum_{i=0}^{k} a_i$, $d_1 = \sum_{i=0}^{k}(ia_i - b_i), d_2 = \sum_{i=0}^{k}\left(\frac{1}{2}i^2 a_i - ib_i\right), \cdots, d_j = \sum_{i=0}^{k}\left(\frac{i^j}{j!}a_i - \frac{i^{j-1}}{(j-1)!}b_j\right)$. As described in [5], $0 = d_0 = d_1 = \cdots = d_m$. The order of the method is the natural number m such that $0 = d_0 = d_1 = \cdots = d_m \neq d_{m+1}$.

In order to define the local truncation error (see [6, P 302-307]), write the exact solution as $x(t_{j+1}) = x(t_j) + \int_{t_j}^{t_{j+1}} x'(t)\,dt$. If $x \in C^m$ then by Taylor's Theorem we can write $x'(t) = P(t) + R(t)$ where $R(t) = \frac{x^{(m+1)}(\xi)}{(m)!}w(t)$ and $P(t)$ is an $(m-1)$-degree polynomial defined as $P_{m-1}(t) = L_{m-1}(t)x'(t_j) + \cdots + L_0(t)x'(t_{j+1-m})$ for m nodes $t_{j+1-m}, \cdots, t_j$ on $[t_j, t_{j+1}]$ where $L_k(t) = \dfrac{\prod_{i=0, i\neq k}^{m-1}(t - t_{j+1-m+1})}{\prod_{i=0, i\neq k}^{m-1}(t_{j+1-m+1} - t_{j+1-m+i})}$ for $k = 0, \cdots, m-1$ and $w(t) = \prod_{i=0}^{m-1}(t - t_{j+1-m+1})$.

Then $\int_{t_j}^{t_{j+1}} x'(t)dt = \int_{t_j}^{t_{j+1}} P_{m-1}(t)dt + E_j$ where $E_j = \int_{t_j}^{t_{j+1}} \frac{x^{(m+1)}(\xi(t))}{m!} w(t)dt$. Using the substitutions $t = hs + t_j$ and $t_k = a + kh$ with the Mean Value Theorem, $E_j = \frac{x^{(m+1)}(\xi_j)}{m!} \int_{t_j}^{t_{j+1}} w(t)dt = \frac{h^{m+1} x^{(m+1)}(\xi_j)}{m!} \int_0^1 s(s+1)\cdots(s+m-1)ds$. Express the local truncation error as

$$\tau_{j+1}(h) = \frac{1}{h}\left(x(t_{j+1}) - x(t_j) - \int_{t_j}^{t_{j+1}} P_{m-1}(t)dt\right)$$
$$= \frac{1}{h}\left(\int_{t_j}^{t_{j+1}} x'(t)dt - \int_{t_j}^{t_{j+1}} P_{m-1}(t)dt\right)$$
$$= \frac{E_j}{h} = \frac{h^m x^{(m+1)}(\xi_j)}{m!} \int_0^1 s(s+1)\cdots(s+m-1)ds = \mathcal{O}(h^m).$$

Looking at the result of a single integration step and assuming no error introduced from previous steps, the error is $\epsilon_1 = \delta$ where δ is the local truncation error of an iteration. In the case of the explicit Adams-Bashforth methods, this error is proportional to h^m where m is the order of the method. The following iteration introduces its own error and when this is accumulated with the error in the previous step, the total error is $\epsilon_2 = \delta + e^{\lambda h}\epsilon_1 = \delta + e^{\lambda h}\delta$. Notice the errors are not simply summed, as the error in the current step critically depends on the error in the previous. The third iteration has error $\epsilon_3 = \delta + e^{\lambda h}\epsilon_2 = \delta + e^{\lambda h}(\delta + \delta e^{\lambda h})$. The relationship is defined by $\epsilon_n = \delta \sum_{i=0}^{n-1} e^{i\lambda h}$. This represents an upper bound on the global truncation error, such that the error ϵ_n does not exceed $\delta \frac{e^{\lambda t_n} - 1}{e^{\lambda h} - 1}$. If the local truncation error is $\mathcal{O}(h^m)$ then the global truncation error is $\mathcal{O}(h^{m-1})$, since $\frac{e^{\lambda t_n}-1}{e^{\lambda h}-1} = \frac{e^{\lambda t_n}-1}{(1+\lambda h+\frac{1}{2}(\lambda h)^2+\cdots)-1} = \frac{1}{\lambda h}(\frac{e^{\lambda t_n}-1}{1+\frac{1}{2}}(\lambda h)+\cdots) \approx \mathcal{O}(h^{-1})$. This leads to $\epsilon_n \approx \mathcal{O}(h^m)\cdot\mathcal{O}(h^{-1}) = \mathcal{O}(h^{m-1})$.

The global truncation error, given by the difference $x_i - x(t_i)$ puts a limit on the accuracy of a puncture point generated by the intersection of Γ with $\mathcal{T}$. In other words, a puncture point on $\mathcal{T}$ has accuracy proportional to a power of the step size h as described above. It is worth noting at this point that the strategy outlined in later sections depends directly on the size of the area around each puncture point which ultimately in turn depends on the step size used to calculate the fieldline.

To describe the stability of the method, differentiate $\frac{dx}{dt} = f(x)$ with respect to $s, x(0) = s$ giving $\frac{\partial}{\partial s}\frac{\partial x}{\partial t} = \frac{\partial}{\partial t}\frac{\partial x}{\partial s} = \frac{\partial f}{\partial x}\frac{\partial x}{\partial s}$ and $\frac{\partial x}{\partial s}(0, s) = 1$. For simplicity, set $u = \frac{\partial x}{\partial s}$. Then $u' = f_x \cdot u$ and $u(0) = 1$. If $\alpha(t) = \lambda - f_x(t)$, then $\alpha(t)$ is a positive function leading to $\frac{u'}{u} = f_x = \lambda - \alpha(t)$ and $\frac{d}{dt}(\ln|u|) \leq \lambda - \alpha(t)$. Now integrate between 0 and t to get $\ln|u(t)| - \ln|u(0)| = \lambda t - \int_0^t \alpha(t)\,dt$ and finally $\ln|u(t)| < \lambda t$ or $|u(t)| < e^{\lambda t}$.

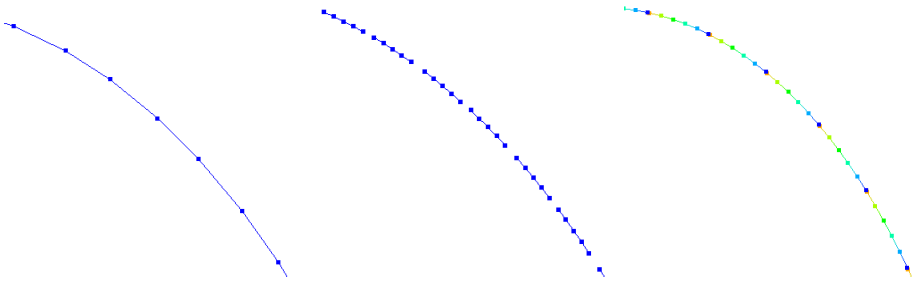

Figure 6: **Left:** An example of a rational surface profile section *before* additional points on the surface were found. **Center:** The same section, *after* adding additional points calculated using the method described. **Right:** A quasi-periodic surface with similar winding group spacing. Color indicates the ordering within a winding group. Notice that successive points in the same winding group 'fill in' the gaps.

This leads to the conclusion that the fieldlines solved with initial values s and $s+\delta$ differ at time t by at most $|\delta|e^{\lambda t}$ since by the Mean Value Theorem, we get $|x(t,s) - x(t,s+\delta)| = |\frac{d}{ds}x(t+\theta\delta)||\delta|$ for some $\theta \in [0,1]$ and $|\frac{d}{ds}x(t+\theta\delta)||\delta| \equiv u(t+\theta\delta)|\delta| < |\delta|e^{\lambda t}$.

3 Strategy

3.1 Overview

The collection of puncture points made by intersecting a rational fieldline with a Poincaré section of the toroidal magnetic field is used to strategically generate new seed points such that the puncture points of the resulting ensemble of rational fieldlines yield a more complete profile of the rational surface. (See Figure 6).

The euclidean distance between successive intersections is used as the minimization value, as fieldlines lying just near a rational surface will have vanishingly smaller distances between a given intersection and the intersection after a toroidal winding number of toroidal windings until the fieldline is right on the surface. The points that have minimized to the surface are drawn in sequence.

The strategy starts by numerically selecting two adjacent puncture points $P_{(max)}$ and $P_{((max+wgo) \mod n_T)}$ made by fieldlines lying on the rational surface intersecting the toroidal plane. These points bound a section of the rational which lies adjacent to the puncture point P_{max} where subscript denotes intersection ordering. The winding group offset of the orbit is signified by wgo which is a useful factor derived from the Blankenship property (see [1, P 5-6])

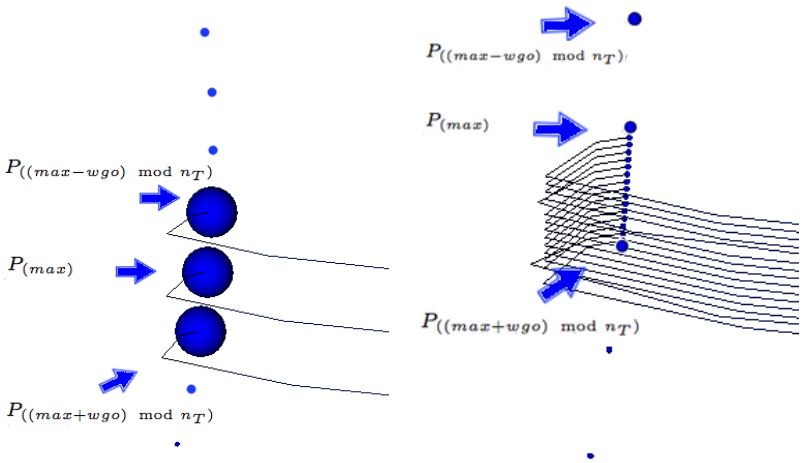

Figure 7: **Left:** A section of a rational surface showing three fieldlines with their respective three points emphasized which, for this curve, turn out to be its $P_{((max-wgo) \mod n_T)}$, $P_{(max)}$ and $P_{((max+wgo) \mod n_T)}$. All three points are used in determining where to place seeds between just two of them. **Right:** The same three points zoomed in somewhat, shown with the newly seeded fieldlines and their respective punctures. This is an example of a best case– the seeds already lie on the surface and the search is complete. That is a coincidence, however, as the position of the points is derived from an arc of a circle built to contain the two bounding rational points plus a third, $P_{((max-wgo) \mod n_T)}$, in both of these images it is the topmost point. When the fieldlines of these new seeds are integrated, puncture points from later winding groups fill in all the gaps between each adjacent pair of the other rational points. Here, $P_{((max+wgo) \mod n_T)}$ and $P_{((max) \mod n_T)}$ are slightly emphasized to show that they border the new seeds.

that gives the number of toroidal windings between winding groups which occur physically adjacent to each other but are not necessarily adjacent in the winding order. Finally, max is the index of the puncture point which forms the largest angle with itself and its two neighbors $P_{((i-wgo) \mod n_T)}$ and $P_{((i+wgo) \mod n_T)}$ $\forall i \in \mathbb{I} : 0 \leq i < n_T$ (See Figure 7). If a sufficient number of new points are inserted on the rational surface evenly between these two points, the result is a smoother approximation of the surface profile. However, if the precise location of the rational surface between these two points were known, then we'd already have those data and a search would be unnecessary. Therefore, an educated guess is made as a starting point.

3.2 Seeding & Bracketing

An arc of the circle connecting the points $P_{((max-wgo) \mod n_T)}$, $P_{(max)}$ and $P_{((max+wgo) \mod n_T)}$ is used to place new seed points $P^*_{A,0}$, $P^*_{A,1}$, $P^*_{A,2}$, ..., $P^*_{A,N}$ for the simulation, where $N+1$ is the number of seeds points desired and A is a label indicating the order of the point for bracketing (See Figure 7). It is assumed that fieldlines generated from points lying on this arc are nearer to the rational surface than those generated from points lying on a chord between existing rational puncture points. These new seeds are in many cases an excellent first approximation, exceeding our tolerance requirement right away and are accepted as lying on the surface. This is frequently the case with higher order rational surfaces, as the approximation is already quite good compared to low order surfaces. Nevertheless, the chord between the two rational puncture points bounding our placement of new seeds is used to generate the second of three points needed for the rest of the procedure, $P^*_{C,0}$, $P^*_{C,1}$, $P^*_{C,2}$, ..., $P^*_{C,N}$. In particular, these points are generated on the intersection of the chord between $P_{(max)}$ and $P_{((max+wgo) \mod n_T)}$ with a line formed perpendicular to it passing through $P^*_i, 0 \leq i < N+1$. The third points, $P^*_{B,0}$, $P^*_{B,1}$, $P^*_{B,2}$, ..., $P^*_{B,N}$, are chosen as the midpoint between $P^*_{A,i}$ and $P^*_{C,i}$ $\forall i \in \mathbb{I} : 0 \leq i < N+1$ (See Figure 8). From here on out, i is used as a subscript to indicate for each point, in order, corresponding to the i^{th} seed, $\forall i \in \mathbb{I} : 0 \leq i < N+1$.

With a set of three new points for each additional point we want to have minimized down to the rational surface, we are ready to establish whether the surface is actually contained somewhere between them. This is done by evaluating the minimization parameter for each new point and comparing them. We shall identify this parameter as $d_{\mathcal{X},i}$ for the distance between the corresponding intersection of i^{th} seed in the $\mathcal{X}^{th}$ minimization stage, and the intersection from that same curve n_T toroidal windings later.

In the first stage, we are bracketing the minimum. This means that we search for a set of three points such that $d_{\mathcal{B},i} < d_{\mathcal{A},i}$ and $d_{\mathcal{B},i} < d_{\mathcal{C},i}$. When this

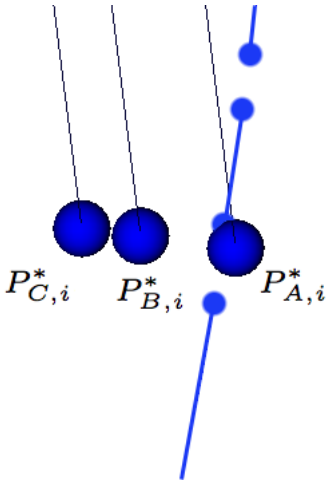

Figure 8: A closely zoomed section of a rational surface shown with three points, from left to right: $P^*_{C,i}$, $P^*_{B,i}$ and $P^*_{A,i}$. These points are in the first iteration of bracketing the minimum, as such $P^*_{A,i}$ here is the seed planted, or the best initial guess from the previous stage. Notice its close proximity to the surface, as well as the spacing between its winding groups. The actual ratio of the chords between the positions of the bracketing points in the first iteration doesn't matter, as the algorithm quickly adjusts it to the golden ratio.

condition is met, the rational surface must lie between $P^*_{A,i}$ and $P^*_{C,i}$, as its d value would be precisely zero (or within precision) if the point lies directly on it. As there cannot be negative distances a d value within error of zero on the rational surface *is* the minimum, and the target of our search (See Figure 9). In the end, we just need a point with a minimization value less than that of both its neighbors to be able to define the neighbors as the bounds or *bracket* on the minimum. Often, our minimum is bracketed right away and we can move directly into the next phase of the search.

When it is not and we must extend our search, $d_{\mathcal{B},i}$ & $d_{\mathcal{A},i}$ are evaluated. If $d_{\mathcal{B},i} > d_{\mathcal{A},i}$, $P^*_{A,i}$ and $P^*_{B,i}$ must be renamed and reordered such that $d_{\mathcal{B},i} < d_{\mathcal{A},i}$. Once this is done, if the minimum is still not bracketed, the search continues by choosing a new $P^*_{C,i}$ until either the minimum has been bracketed or no minimum can found. A new $P^{**}_{C,i}$ to replace the last one is calculated by extending the chord from $P^*_{B,i}$ to the old $P^*_{C,i}$ by a fixed ratio; in this case we use the golden ratio [3, P 491]. Finally, $P^{**}_{C,i}$ is relabeled as $P^*_{C,i}$, completing one iteration of the bracketing loop. Notice that depending on whether $P^*_{A,i}$ and $P^*_{B,N}$ must be swapped, the search may proceed in opposite directions at different points along the chord between $P_{(max)}$ and $P_{((max+wgo) \mod n_T)}$.

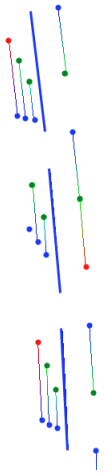

Figure 9: This image shows a bracketed rational surface as a blue line. The colored lines to the left of the rational show curves with progressively smaller gaps between puncture points of the same toroidal winding group, the basis for the minimization. The color indicates winding order. The line to the right of the rational is there to indicate the reversal of the direction of the winding, characteristic of regions on either side of a rational surface. Three of the fieldlines were seeded at points used for the first iteration of bracketing.

3.3 Minimization

When the rational surface has been bracketed, the next phase of the search begins [3, P 495-496]. Points $P^*_{A,i}$ and $P^*_{C,i}$ are relabeled $P^*_{X0,i}$ and $P^*_{X3,i}$, respectively. Point $P^*_{B,i}$ is relabeled $P^*_{X2,i}$ if the length of the vector V_{AB} from $P^*_{A,i}$ to $P^*_{B,i}$ is greater than the length of the vector V_{BC} from $P^*_{B,i}$ to $P^*_{C,i}$, and it is labelled $P^*_{X1,i}$ if $||V_{BC}|| > ||V_{AB}||$. This provides more space for the fourth of four points needed for the minimization routine (See Figure 10). This last point is calculated to be some distance between the two with the largest gap– the distance is determined such that the golden ratio applies to the resulting line segments between the new point and its neighbors. Once $P^*_{X0,i}$, $P^*_{X1,i}$, $P^*_{X2,i}$ and $P^*_{X3,i}$ have been designated and their corresponding fieldlines have been integrated, $d_{X1,i}$, $d_{X2,i}$ are evaluated. The smaller of the two is nearer to the minimum, which we've previously established lies between $P^*_{X0,i}$ and $P^*_{X3,i}$. Suppose the point with the smaller d was $X2$. Now we know more accurately where the minimum lies, specifically that it lies between $P^*_{X1,i}$ and $P^*_{X3,i}$, since $d_{X2,i} < d_{X1,i}$ from above, and $d_{X2,i} < d_{X3,i}$ from the bracketing routine. If $d_{X2} \leq \delta_{max}$ where δ_{max} is our tolerance limit then $X2$ is also our minimum, and if our tolerance was set correctly $X2$ lies on the rational surface. If $d_{X2,i} > \delta_{max}$ then we now treat $P^*_{X1,i}$, $P^*_{X2,i}$ and $P^*_{X3,i}$ as $P^*_{A,i}$, $P^*_{B,N}$ and $P^*_{C,i}$ respectively and repeat this paragraph. Each iteration resolves to a tighter bound on the minimum and when one of the inner points is better than the tolerance, we take

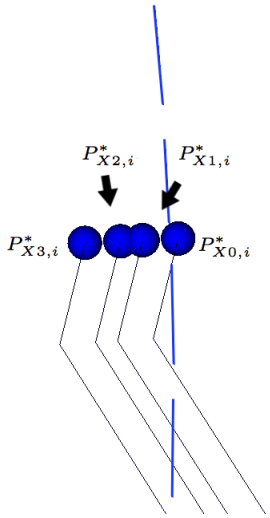

Figure 10: In this figure, the rational surface is shown with four minimization points, three of which were the final bracketing points and the fourth was calculated to fill in the largest gap. Points shown from left to right: $P^*_{X0,i}$, $P^*_{X1,i}$, $P^*_{X2,i}$, & $P^*_{X3,i}$

that point and label it as ready to draw. However, it isn't yet ready to draw until all other seeds have completed their searches.

This entire process is repeated for each seed until the searches have all either failed or succeeded and produced a point on the surface. The ordering of the points is maintained throughout the process and the points are connected in order when drawn, in their respective winding groups (i.e., the groups formed from different windings of the collection of curves).

The ratio used when seeding new bracketing curves or minimizing curves is that of the *golden mean* or *golden section*, allegedly from the ancient Greeks. Each iteration of the technique refines the bounds on the minimum by a factor of .61803 times the previous interval. This is on the order of, but not quite as good as a factor of .50000 that is achieved from a bisection method. The convergence is linear. This ratio was not chosen for its historical significance, but rather it has been derived as the optimal segmenting ratio in order to avert pitfalls of the bisection method [3, p 494].

4 Results & Discussion

The resultant puncture points form a smoother piecewise linear approximation of the complete rational surface (Figure 11). The points lie on the rational

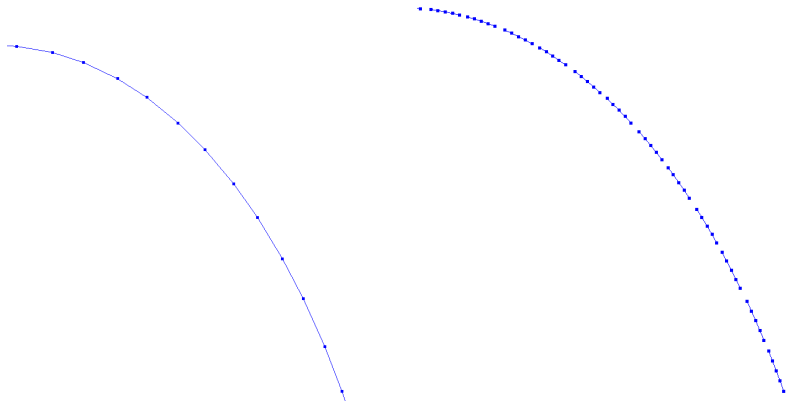

Figure 11: **Left:** Typical piecewise linear approximation of a rational surface. The connected data points are puncture points from a single fieldline. **Right:** The result after following the technique described in this paper: four additional puncture points (and therefore fieldline seed points) on the rational surface for every puncture point in the original.

surface to within either the chosen tolerance if possible, or to the limits imposed by errors in integration. More points on the surface are known than when looking at one rational fieldline, because by definition rational fieldlines do not spread out. Thus, the introduction of additional fieldlines to fill in the gaps of the original achieves the objective of visualizing a rational surface with a level of detail comparable to that available from irrational surfaces afforded them by their progressive behavior.

The algorithm described in this paper is robust, and the minimization routine is guaranteed to converge on the minimum as long as it exists and the behavior of the field is predictable, smooth and monotonic [3, p 492-496]. It is possible the algorithm fails to select the correct rational surface for some of the points if there is more than one minimum in close proximity, as the bracketing routine could inadvertently bracket more than one minimum, and the minimization algorithm could select any of them in the end. In this case, the resultant drawing is of varying quality.

While low order surfaces are of primary interest, many of the surfaces used as test data for this work, and indeed many of the sample results used as figures in this paper are of higher order rational surfaces, which already give much better piecewise approximations than do low order rational surfaces, such as a 2,1. This is partly due to a scarcity of low order rational surfaces in the test data but also due to numerical errors related to precision since such surfaces commonly have a diameter on the same order of magnitude as the limit of precision. The low order rational surfaces tested for this project did not yield good results due to precision issues. Nevertheless, the results on higher order

rational surfaces are very good and it would be reasonable for adjustments to be made to accommodate the difficulties encountered with low order surfaces.

The minimization algorithm used is a common one, and does not converge as rapidly as others. A number of such improved minimization routines are described in later sections of [3]. Additionally, the implementation in VisIt [2] does not leverage its parallel design and as such is strictly serial, and thus not very fast. The implementation could be expanded to utilize this latent power fairly easily, as minimization seeds only depend on other fieldlines in their respective minimization groups, and each group could be numerically integrated individually in parallel.

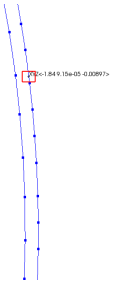

Figure 12: Two curves have been identified as rational surfaces. The left curve is an 80,39, the right is a 119,58.

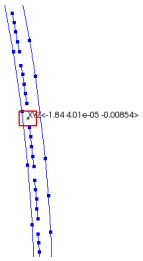

Figure 13: The same two curves but with an additional curve in between, which has had its winding numbers overridden to match the lower order rational.

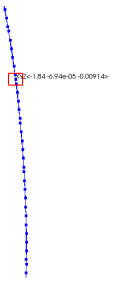

Figure 14: The result of applying the minimization routine to the test seed from Figure 13: The minimization found the lower order surface and added more puncture points to the plot.

4.1 Testing

As a qualitative test of the method's robustness, new fieldlines are seeded near a known rational surface and the result is compared with the expectation (i.e., the seed should minimize to the rational). The further from the rational a seed is planted which successfully minimizes to the rational, the better the robustness. One limitation of this test is that the distance to the next rational surface limits the range of testing input. This distance is determined by the local topology of the field. Nevertheless, as long as each seed is chosen such that no other rational surface lies closer to it (or that the first derivative of the field at that point doesn't slope away from the target rational), the method brackets the target rational and minimizes to it. If the bracketing points are sloped towards the target rational and don't encompass any other critical surfaces, with enough iterations the target rational will eventually be bracketed. A quantitative analysis of the robustness could be performed given a data set with a known lone rational surface, defined as being more than twice as far from another rational

surface than the bounds as defined in section 2.4. In Figure 12, two rational surface profiles are shown. The left surface has a lower, and therefore more stable winding number while the right surface has a slightly higher winding number. A point between the two rational surfaces is chosen as a test seed (see Figure 13). Its analysis is overridden with the winding values of the nearby rational to show the relative spacing of successive punctures in a winding group. The algorithm in this paper is applied to this test seed, and the resulting curve is shown drawn together with the original rational surface in Figure 14. Thus, the method demonstrates robustness within the described testing limitations.

The accuracy of the approach described in section 3 ultimately depends on the accuracy of a calculated fieldline for the factor used to determine its overlap, or its distance in relation to a rational surface. The global error is bounded linearly by a power of the integration step size h. With this in mind, a test was designed and performed in order to describe the quality of the result achieved as a factor of the integration step size. An initial seed is planted in the same location near a known rational surface and the method described in this paper is run for different integration step sizes. In order to control the test, a hard coded number of seeds are generated along the arc between the same two puncture points on the surface found with the original seed. In the results presented here, 11 seed points are used. The control case is chosen as the test with the smallest step size, so that comparing the various test cases against the control gives a meaningful indication of the effect without requiring an arbitrary level of precision. The error is calculated using the absolute distance from each puncture point obtained with a given step size to its counterpart in the control set (which uses a much smaller step size). In other words, the further a point is from its counterpart calculated with a much lower step size, the greater the error accumulated. This test was run at a number of step sizes covering nearly two orders of magnitude. The range of the step sizes tested was selected based on pre-existing knowledge about the error's relationship to the step size and to illustrate the growth pattern of the error. Additionally, it becomes increasingly difficult to obtain results for step sizes beyond the range used. It should be emphasized that the error is *bounded* by an expression which grows linearly with the step size. This explains the wide range of errors obtained, as some seeds continue to achieve better results than others, and it is evident that this performance depends on the rank of the seed along the arc used for their generation. In any case, the results (see Figure 15) show that the error, acknowledging some noise, is indeed bounded linearly as described in section 2.4. In order to more clearly show the values obtained for very low step sizes, a closer view of those results is shown in Figure 16.

An obstacle to both the robustness and accuracy tests, and the approach in general, lies in encountering multiple rational surfaces in close proximity. Additionally, a poor choice in integration step size results in a chaotic looking rational surface as a result of increased local truncation error leading to increased global truncation error. A solution to the first case will not be proposed here

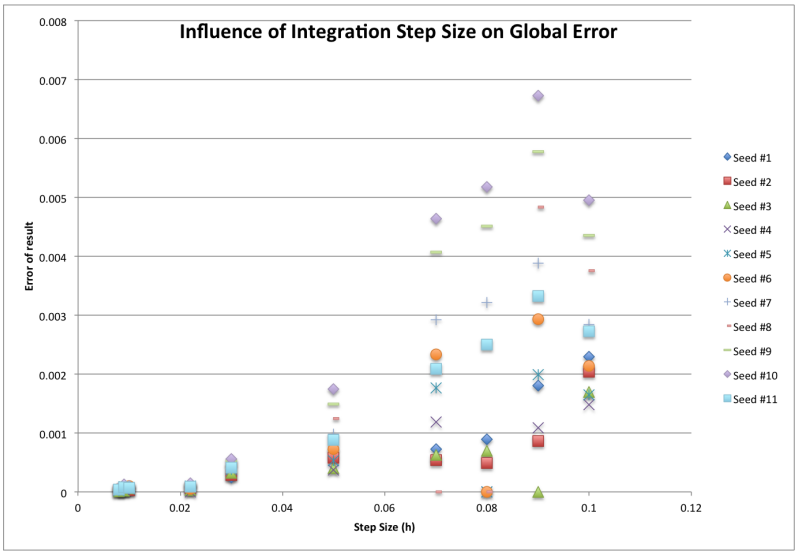

Figure 15: The effect of varying integration step size on the overall error.

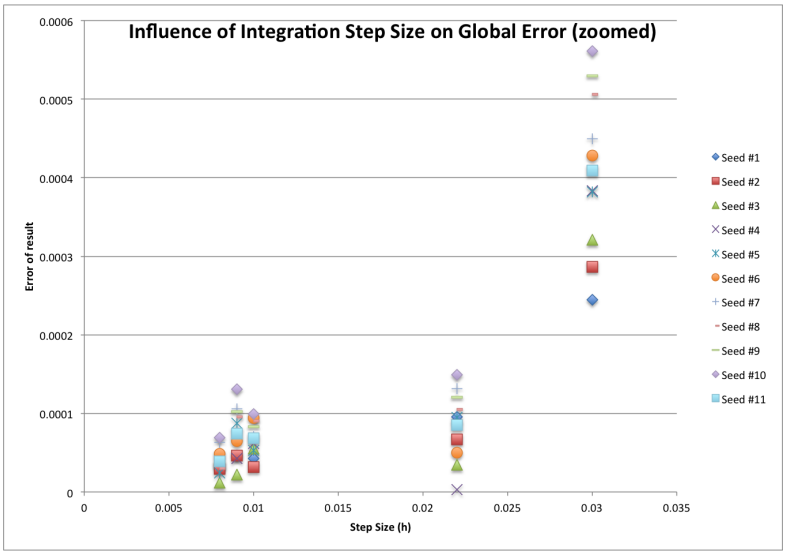

Figure 16: The same data as in the first few columns of Figure 15, presented for clarity.

beyond choosing seed points carefully together with the solution to the second case, which is to verify the integration step size is chosen appropriately.

5 Conclusions

It has been demonstrated that additional data points on a given rational surface in a toroidal magnetic field can be searched and found numerically. Rational surfaces are of particular interest because it is from rational surfaces that island chains form, and until now their very nature hindered their complete elucidation. A working implementation has been deployed as a plugin for VisIt in C++ and the source code is available publicly.

While this work demonstrates the value of a numerical minimization in the context of toroidal vector field simulations, the minimization technique employed is a simple one that could be improved with, e.g., a parabolic interpolation. Consequently the algorithm developed and implemented here makes no claims of optimality. In any case, the viability of the technique has been demonstrated. Future work, in addition to improvements to this work, might entail tracking the rational surfaces through time, or its islands as they form.

6 Acknowledgements

The author would like to thank Allen Sanderson for providing the opportunity, his professional guidance and his technical assistance, Mike Kirby for his academic guidance and Chris Johnson for his guidance and academic support. Thanks to Savannah for being so patient and for all the homebrew– you are my motivation.

References

[1] Sanderson, Chen, Tricoche, Pugmire, Kruger, Breslau - Analysis of Recurrent Patterns in Toroidal Magnetic Fields, 2010.

[2] Visit visualization tool, http://www.llnl.gov/visit

[3] Press, Teukolsky, Vetterling, Flannery – Numerical Recipes - Cambridge University Press, 3rd Edition, 2007.

[4] J. Hale and H. Kocak. Dynamics and Bifurcations – New York - Springer-Verlag, 1991.

[5] David R. Kincaid and E. Ward Cheney – Numerical Analysis: Mathematics of Scientific Computing - Brooks Cole, 2nd edition, 1996.

[6] Richard L. Burden, J. Douglas Faires – Numerical Analysis - Cengage Learning, 9th edition, 2010.